Langmuir

Article

pubs.acs.org/Langmuir

Periodic Ice Banding in Freezing Colloidal Dispersions

Anthony M. Anderson* and M. Grae Worster

Department of Applied Mathematics and Theoretical Physics, University of Cambridge, Wilberforce Road, Cambridge CB3 0WA, United Kingdom

Supporting Information

ABSTRACT: Concentrated colloidal alumina dispersions were frozen in a directional solidification apparatus that provides independent control of the freezing rate and temperature gradient. Two distinct steady-state modes of periodic ice banding were observed in the range of freezing rates examined. For each mode, the wavelength between successive bands of segregated ice decreases with increasing freezing rate. At low freezing rates (0.25−3 μm s^{-1}), the ice segregates from the suspension into ice lenses, which are cracklike in appearance, and there is visible structure in the layer of rejected particles in the unfrozen region ahead of the ice lenses. In this regime, we argue that compressive cryosuction forces lead to the irreversible aggregation of the rejected particles into a close-packed cohesive layer. The temperature in the aggregated layer is depressed below the bulk freezing point by more than 2 °C before the ice lenses are encountered; moreover, this undercooled region appears as a light-colored layer. The magnitude of the undercooling and the color change in this region both suggest the presence of pore ice and the formation of a frozen fringe. The possibility of a frozen fringe is supported by a quantitative model of the freezing behavior. At intermediate freezing rates, around 4 μm s^{-1}, the pattern of ice segregation is disordered, coinciding with the disappearance of the dark- and light-colored layers. Finally, at high freezing rates (5−10 μm s^{-1}), there is a new mode of periodic ice banding that is no longer cracklike and is absent of any visible structure in the suspension ahead of the ice bands. We discuss the implications of our experimental findings for theories of ice lensing.

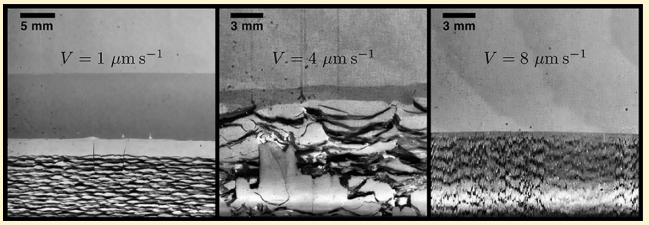

INTRODUCTION

The freezing of colloidal suspensions is a process that impacts technological applications and the natural environment alike. One particularly important observation is that colloidal suspensions do not freeze uniformly: the frozen phase (e.g., ice) becomes segregated, trapping bulk regions of colloid within and generating a rich set of patterns.[1−5] A process known as "freeze-casting" utilizes this phenomenon in a versatile processing route for the fabrication of bioinspired porous materials and composites.[3,6,7] Other technological applications include cryobiology,[8,9] food engineering,[10] and soil remediation.[11] In nature, ice segregation underlies frost heave, whereby saturated soils expand as they freeze,[1,2] which can lead to beautifully patterned ground in regions of permafrost[12] but also promotes erosion and causes damage to manmade structures.[13] A major goal in understanding all of these systems is to elucidate the physical processes by which ice becomes segregated in order to predict the conditions under which the various patterns occur.

Studies that have focused on the interaction of an isolated particle with a solidification front have contributed greatly to our understanding of the essential physics behind ice segregation.[14−16] There exists a maximum freezing rate below which a particle of a given size is pushed ahead of the freezing front, whereas at higher freezing rates the particle is completely engulfed. The capture rate increases as the particle size decreases owing to an interplay between viscous stresses, which promote capture, and disjoining forces, which maintain a premelted liquid film between the particle and ice.[16,17] A colloidal particle that is smaller than 1 μm in size will typically remain expelled from the ice phase for freezing rates below 10 μm s^{-1}. Although theories of isolated particles help explain the tendency for ice segregation in colloidal systems, all of the applications mentioned above require that these principles be extended to systems of many particles, where the role of particle−particle interactions in ice segregation needs further clarification.

Ice banding is a familiar pattern of ice segregation in concentrated particulate systems that features alternating macroscopic layers of ice and particles that are oriented transverse to the temperature gradient. Since Taber's experiments on frozen soils,[1,2] the appearance of discrete bands of particle-free ice, called ice lenses, has been firmly linked with the phenomenon of frost heave. Similar patterns of ice segregation have also been observed in experiments with colloidal suspensions.[4,5,18,19] Despite the prevalence of these patterns, there is still much uncertainty about the physical processes controlling the formation of ice lenses. The most widely accepted theory for ice-lens formation is given by "rigid-ice" models.[20−22] These models treat the suspension as a rigid

Received: August 28, 2012
Revised: October 30, 2012
Published: October 30, 2012

or elastic porous matrix and reproduce, at least qualitatively, the observations of ice lensing in Taber's experiments. Crucially, ice lensing in rigid-ice formulations requires the existence of a "frozen fringe", which is a region of partially frozen suspension extending beyond the warmest ice lens wherein the succeeding ice lens is initiated. The physical basis for a frozen fringe was clarified by Rempel et al.,[22] who showed that the microscopic interactions between particles and pore ice within the frozen fringe manifest themselves in a thermomolecular pressure gradient that provides a force to cleave the soil and make way for a new ice lens.

To our knowledge, no quantitative experimental tests of rigid-ice models have been reported. Moreover, several studies have challenged the basic assumptions of these models. Watanabe and Mizoguchi[19] observed ice lenses in directional freezing experiments with monodisperse silica particles but could not detect a pore-ice-bearing fringe using Raman spectroscopy. Peppin et al.[4] performed similar experiments with colloidal clay suspensions for a range of initial particle concentrations and observed ice lenses as well as other patterns of ice segregation, including vertically aligned (dendritic) ice crystals and polygonal patterns resembling mud cracks. Spatial variations in the particle concentration due to a buildup of rejected particles were detected in the vicinity of the segregated ice. These colloidal concentration gradients, which are neglected in rigid-ice formulations, can trigger a thermodynamic instability that leads to morphological transitions in the pattern of segregated ice.[23,24] Recently, these thermodynamic principles were extended to cohesive particle systems,[25] giving conditions for the formation of ice lenses through the extension of ice-filled cracks along isotherms, without the requirement of a frozen fringe. Finally, in a set of experiments with alumina exploring much higher freezing rates, Deville and co-workers[5,26] identified a pattern of dendritic ice segregation with intermittent bands of ice. A disequilibrium mechanism based on particle capture was recently proposed to explain the banding,[27] drawing on an analogy with solute banding in rapid alloy solidification.

In light of these uncertainties, we performed controlled freezing experiments with electrostatically stabilized colloidal alumina dispersions. These experiments utilized a directional solidification apparatus that enables independent control of the freezing rate and temperature gradient, similarly to the apparatus used in refs 18 and 19. We report on the quasi-steady patterns of ice segregation obtained for a range of freezing rates at a fixed initial particle concentration. Two distinct modes of periodic ice banding are described. At the lowest freezing rates, the pattern of ice segregation is remarkably cracklike in appearance and is accompanied by a layer of rejected particles visible as light- and dark-colored layers. At the highest freezing rates, this layered structure is absent, and the bands of ice no longer resemble cracks. In these various steady states, it is apparent that the structure of the layer of rejected particles plays a critical role in establishing the mode of ice segregation. On this premise, we provide a detailed examination of the light- and dark-colored layers that make up the boundary layer of rejected particles at low freezing rates. Experimental observations reveal that the rejected particles irreversibly aggregate into a close-packed cohesive layer. It is known from centrifugation[28,29] and drying[30−32] studies that an irreversible destabilization of close-packed particles occurs when compressive stresses exceed electrostatic repulsions. A simple theory is developed to assess the role of compressive cryosuction forces in producing aggregation ahead of a growing sequence of ice lenses. Our findings have important implications for rigid-ice models, as discussed in the final section.

DIRECTIONAL SOLIDIFICATION EXPERIMENTS

A series of freezing experiments were conducted with colloidal alumina suspensions, which were prepared by combining α-alumina powder (Alfa-Aesar, ≥99.95% purity) with deionized water (Millipore AFS-60D). These powders were nearly monodisperse, consisting of particles with an approximately spherical morphology and a mean diameter of 0.32 ± 0.06 μm. The particles had a density of 3.97 g cm^{-3} and a specific surface area of 7.7 m^2 g^{-1}. After the particles had been combined with water to produce a mixture with 60 wt % (27 vol %) alumina, the suspensions were adjusted to pH 5 with a stock solution of analytical-grade HCl and then pulsed with an ultrasonic probe (Branson Sonifier 250) at 20 kHz for 5 min to fully disperse the particles and break up any remaining agglomerates. Before the samples were frozen, they were equilibrated for at least 12 h, ultrasonicated for another minute, and finally readjusted to pH 5 with HCl. This procedure was adapted from a protocol used previously to prepare alumina suspensions in rheological[33] and drying[34] experiments. With α-alumina having an albedo near unity, the suspensions resulted in an opaque white liquid, similar to milk.

No additional salt was used to prepare the samples; only HCl was used. This choice was made to avoid, as much as possible, the complicating effects that impurities have on the freezing behavior of water; however, some amount of HCl was needed to adequately disperse the particles. The dependence of the zeta potential, ζ (an indicator of the surface charge on the suspended particles), on the pH of α-alumina suspensions is known from electrophoresis measurements (e.g., ref 33), which are reproduced in Figure 1. The isoelectric point (IEP, ζ = 0) occurs at approximately pH 9, and a maximum (positive) ζ value is obtained at approximately pH 4. The modulation of the

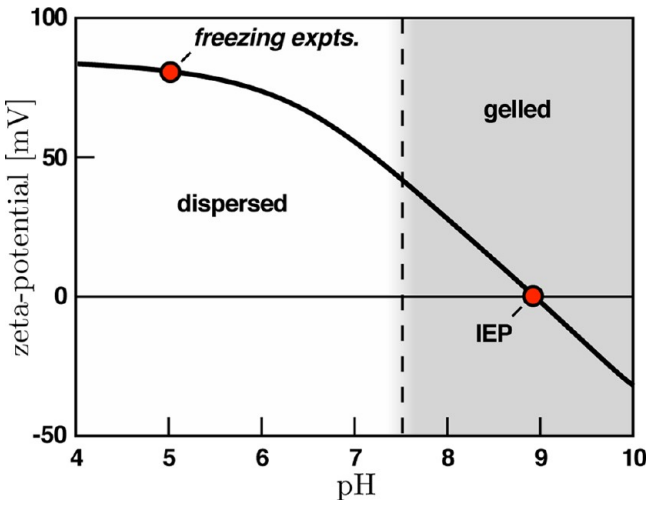

Figure 1. Dependence of the zeta potential on pH in an α-alumina suspension, reproduced from electrophoresis measurements in ref 33 to illustrate the essential features: The isoelectric point (IEP) and maximum (positive) value occur at pH ≈ 9 and pH ≈ 4, respectively. For a 60 wt % (27 vol %) particle concentration, a gel transition was observed at pH ≈ 7.5 (dashed line). Freezing experiments were performed with stable dispersions at pH 5.

dx.doi.org/10.1021/la303458m | Langmuir 2012, 28, 16512−16523

electrostatic particle interactions over this range of pH leads to stable dispersions at low pH and flocculated suspensions at pH values centered around the IEP, which can form gels. For the 27 vol % particle concentration used here, a sharp transition was observed between a liquid and a gelled suspension (with the consistency of facial cream) at a pH value of approximately 7.5 (see Figure 1), which is in line with the value inferred from previous rheological measurements.[33] Here, the value pH 5 was chosen to obtain highly stable dispersions. Stability was important, because, in a few instances, freezing experiments were allowed to run for several days. By setting a portion of each sample aside in a test tube, we observed negligible sedimentation in the reserved unfrozen samples over the duration of the freezing experiments.

The prepared samples were frozen in the directional solidification facility shown in Figure 2. The samples were

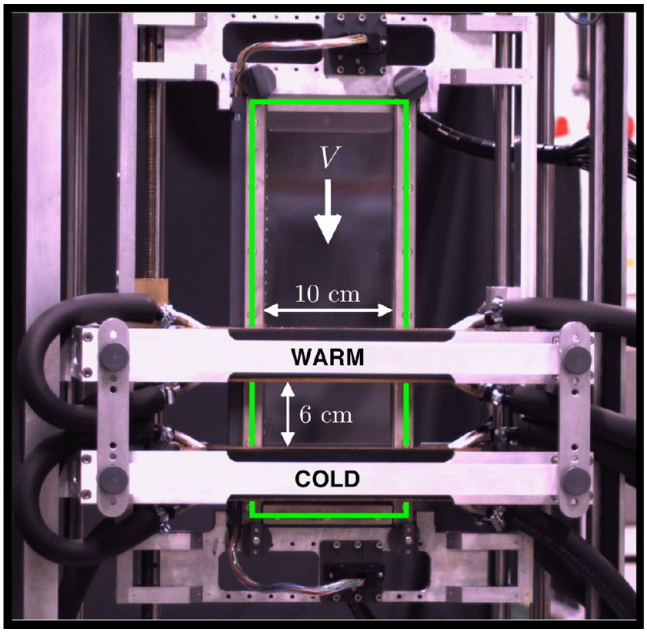

Figure 2. Directional solidification apparatus. The suspensions are loaded into a Hele-Shaw cell (38 × 10 × 0.3 cm, highlighted in green) that is pulled at speed V through a fixed temperature gradient set by two heat exchangers (labeled warm and cold) separated by 6 cm. The entire apparatus is enclosed in a cabinet (not shown) through which dry air is circulated to prevent condensation. A digital camera was focused on a region directly above the cold plate to record time-lapsed images of the freezing suspensions.

loaded into a Hele-Shaw cell, with inner dimensions 38 × 10 × 0.3 cm^3 between 2-mm-thick Pyrex glass plates held together by, but thermally insulated from, an aluminum frame. The cell was sandwiched between two brass heat exchangers in direct contact with the glass, enabling control of the temperature gradient along the length of the cell. Each heat exchanger was connected to a dedicated cooler that pumped ethylene glycol through the brass blocks in order to maintain the temperature. An outer frame held the cell in position and was attached to a screw driven by a microstepper motor so that the cell could be translated downward at a controlled pulling speed V through the fixed temperature gradient. In some experiments, a thermistor was inserted along the center of the cell to record the temperature profile. The entire apparatus was enclosed in a glass cabinet supplied with dry air (20−22 °C) to prevent condensation and enable the freezing to be monitored with time-lapse images taken with a digital camera focused on a region directly above the cold plate.

With this configuration, quasi-two-dimensional macroscopic samples can be frozen with precise control of the freezing rate and temperature gradient, thus providing a geometry that is amenable to theoretical analysis. In all of the experiments described herein, the temperatures of the upper and lower heat exchangers were fixed at 0.5 and −15 °C, respectively. The focus of this article is on the steady-state freezing morphologies obtained for pulling speeds between 0.25 and 10 $\mu m\ s^{-1}$. Depending on the pulling speed, the time required to reach steady state once the cell was put in motion was between several minutes ($V = 10\ \mu m\ s^{-1}$) and a couple of days ($V = 0.25\ \mu m\ s^{-1}$). The images obtained from these experiments are discussed in the next section.

QUASI-STEADY ICE SEGREGATION PATTERNS

Images of the frozen suspensions at steady state are shown in Figure 3 for several pulling speeds. All of the images display a region of the suspension directly above the lower heat exchanger, where the temperature was set at −15 °C. Here, the segregated ice appears black, and the colloid appears in shades of gray. Because these images were taken in a frame of reference attached to the cooling plates, new material from the bulk suspension above was continuously being fed down toward the freezing zone at the prescribed pulling speed. Consequently, to preserve a steady state, particles that were not rejected and pushed ahead at the freezing front became trapped between adjacent regions of segregated ice and eventually swept away out of the frame of view: New layers of segregated ice continually formed and entrained particles at the freezing front. For this reason, we refer to the ice segregation patterns as quasi-steady. Supporting movies are provided for pulling speeds of $V = 1$, 4, and 8 $\mu m\ s^{-1}$, showing the freezing suspensions as they approach steady state (see Movies S1−S3, Supporting Information).

The freezing behavior can be classified according to pulling speed following the arrangement of the images in Figure 3: low (a−c), intermediate (d−f), and high (g−i). For both low and high freezing rates, the ice segregates into spatially periodic bands oriented transverse to the freezing direction, and the spacing between successive bands is observed to decrease with increasing pulling speed. The freezing behavior in these two regimes is markedly different however, and there is a transition between the two modes of ice banding at the intermediate freezing rates, which is most readily apparent at $V = 4\ \mu m\ s^{-1}$, where the pattern of ice segregation is highly disordered. For low freezing rates, 0.1−2 $\mu m\ s^{-1}$, the ice bands appear remarkably cracklike and are reminiscent of ice lenses found in freezing saturated soils and rocks. An incipient ice lens emerges as a small fracture that expands horizontally and gradually thickens (see Movies S1 and S4, Supporting Information). Vertical ice-filled cracks are also observed that extend beyond the warmest ice lens. These vertical cracks are likely of the same origin as those observed by Chamberlain and Gow[35] in frozen clays and appear similar to the shrinkage cracks found in drying colloidal suspensions.[31,32,34,36,37] Once a vertical crack is established, it can propagate over several generations of ice lenses (see Figure 3a) before the tip of the crack is deflected back toward the ice lenses and left behind by the freezing front (see Figure 3d, bottom left corner). However, the vertical cracks are not a ubiquitous feature, and the formation of

dx.doi.org/10.1021/la303458m | Langmuir 2012, 28, 16512−16523

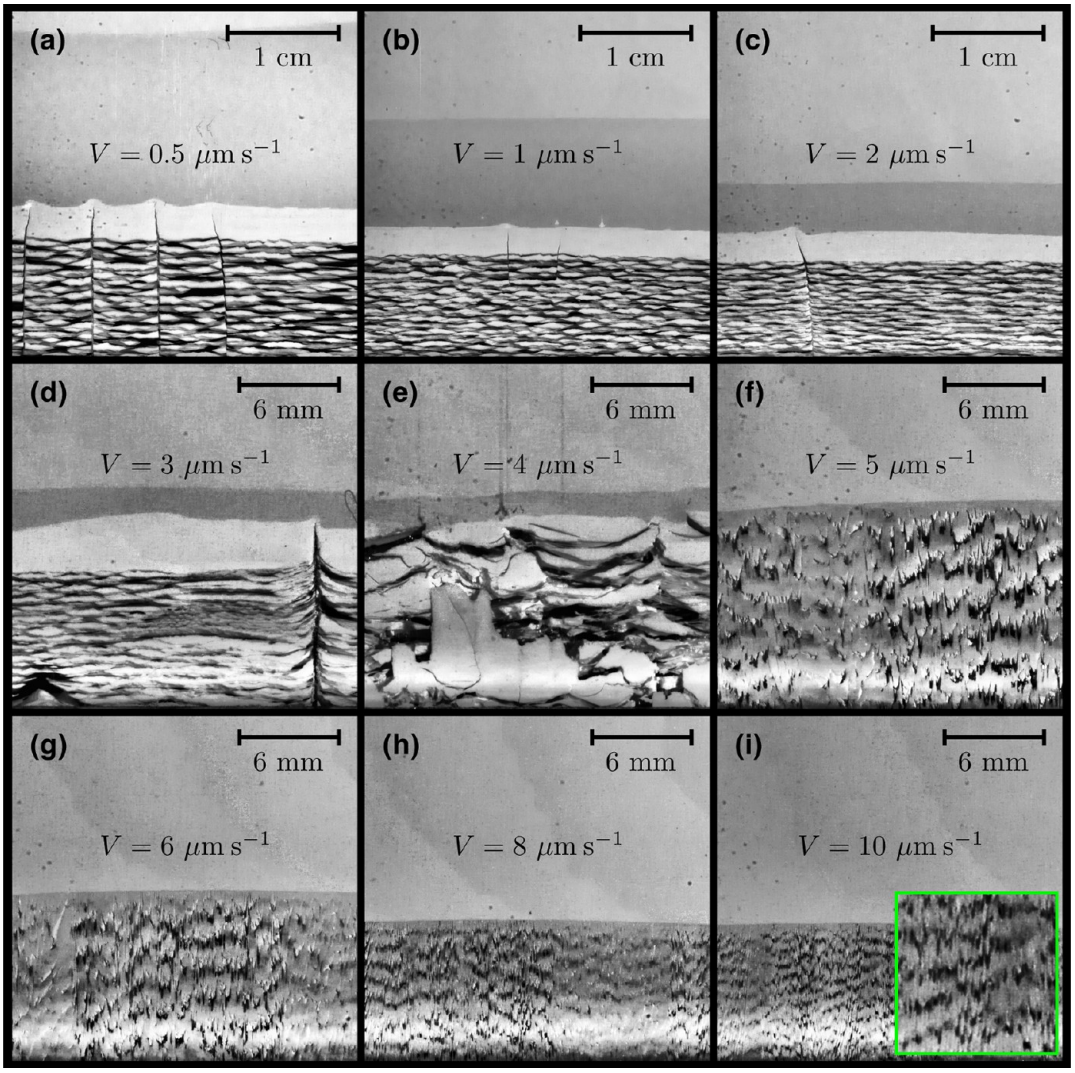

Figure 3. Quasi-steady ice segregation patterns for a range of pulling speeds. The images display a region immediately above the cold plate; segregated ice appears black, and colloid appears gray. (Note that the bright band at the bottom of images d–i is a reflection from the lower brass heat exchanger.) (a–c) Slow and (g–i) fast freezing produced distinct modes of periodic ice banding, each mode having a bandwidth that decreased with increasing pulling speed. A transition between the two modes of ice banding occurred at (d–f) intermediate freezing rates, signaled by (e) disordered ice segregation at $V = 4\ \mu m\ s^{-1}$. The ice bands are cracklike in the slow regime, resembling ice lenses in frozen soils and rocks, and are accompanied by dark and light layers, situated between the bulk suspension and the region of segregated ice. The dark layer has a glassy sheen when viewed with the naked eye. Vertical ice-filled cracks can also be observed in this regime, for example, in panel a. In the fast regime, the ice bands are highly modulated along the horizontal axis, producing a wavy and jagged appearance (see inset in panel i). The suspension appears uniform all the way down to the region of segregated ice at high freezing rates.

horizontal lenses does not appear to depend on them. For high freezing rates, 6–10 $\mu m\ s^{-1}$, the ice bands no longer appear as cracks. The ice bands in this regime are highly modulated in the horizontal direction, which produces a waviness on the order of about 1 mm. On a smaller scale, thin vertical streaks of colloid can be seen intersecting the bands, giving them a jagged appearance (see inset to Figure 3i).

The visible structures of the suspension ahead of the freezing front are markedly different for the two modes of ice banding. For high freezing rates, the suspension appears to remain uniform all the way to the freezing zone, whereas for low freezing rates the suspension is layered: Light- and dark-colored layers are formed between the bulk suspension and the region of segregated ice. The thickness of the darker layer decreases with increasing pulling speed, whereas the thickness of the light layer is relatively insensitive to the pulling speed up to $V = 4\ \mu m\ s^{-1}$, the speed at which it no longer appears as a continuous layer separated from the region of segregated ice (see Figure 4). When vertical ice-filled cracks are present, the vertical extent of the cracks coincides with the vertical extent of the light layer, and the boundary between the light and dark layers becomes deformed in the vicinity of the crack tips. Based on these observations, it would seem that these dark and light layers play an integral role in ice banding. In the next section, further experimental observations are presented to identify the nature of these layers in the suspension and to characterize the subsequent ice lensing in the slow freezing regime.

■ PARTICLE AGGREGATION AND ICE LENSING

Further Experimental Observations. Temperature profiles in steady state were measured using a thermistor fixed with respect to the cell and translated along the freezing axis

dx.doi.org/10.1021/la303458m | *Langmuir* 2012, 28, 16512–16523

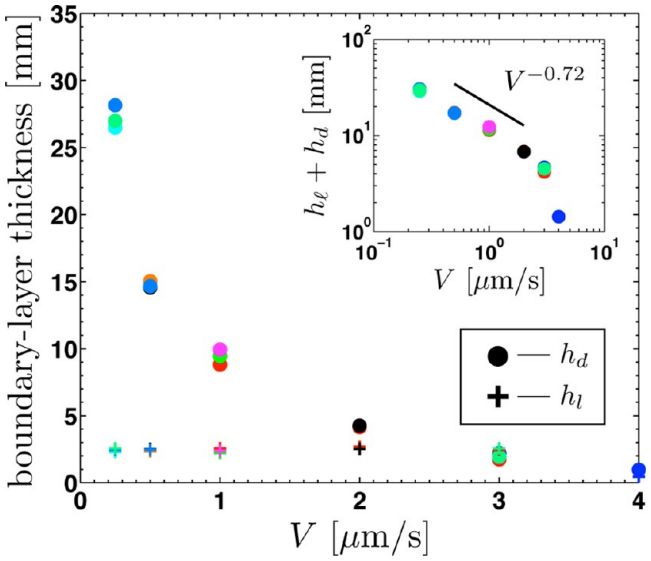

Figure 4. Measured thicknesses of the dark (h_d, circles) and light (h_l, crosses) boundary layers versus pulling speed. The different colors refer to separate experiments, confirming that the measurements were not subject to hysteresis. The value of h_d varies appreciably with V, whereas the value of h_l is relatively insensitive to V, remaining approximately constant at 2.5 mm. The sum of h_d and h_l, giving the total thickness of the aggregated layer, was found to depend on pulling speed as $V^{-0.72}$ (inset) up to $V = 3$ μm s^{-1}, after which a transition away from ice lensing occurred.

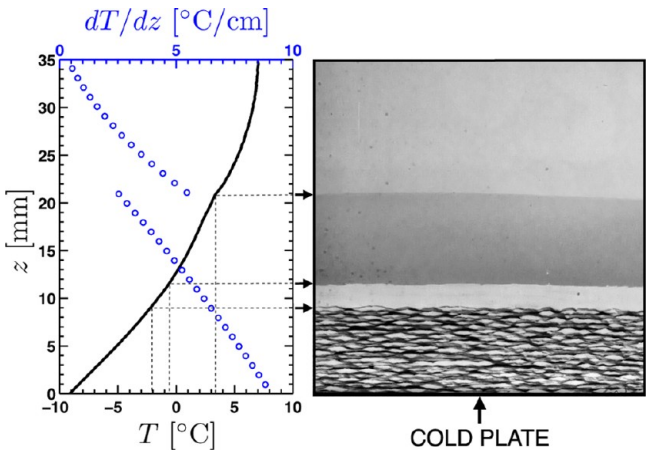

Figure 5. Photograph of a frozen sample with its corresponding vertical temperature profile measured along the freezing axis in steady state ($V = 1$ μm s^{-1}). The solid black curve (bottom axis) is the temperature $T(z)$, and the open blue circles (top axis) are the temperature gradient $T'(z)$, computed from a continuous piecewise polynomial fit of $T(z)$. The leading edge of the light intermediate layer resides below the isotherm of the bulk freezing temperature (0 °C). The jump in the temperature gradient at warmer temperatures coincides with the leading edge of the dark layer and is the result of an abrupt change in particle concentration.

between the two heat exchangers. Because the pulling speed V is known and steady, the resulting temporal trace of the temperature can be mapped onto the vertical axis. A typical temperature profile is shown in Figure 5 alongside an image of the freezing sample ($V = 1$ μm s^{-1}). There are two important features to note. First, the isotherm for the bulk freezing point, 0 °C, resides above the boundary between the dark and light layers in the suspension and the first instance of segregated ice occurs once the temperature is cooled below the bulk freezing point by nearly 2 °C. As the pulling speed is varied, the temperature at the warmest ice lens remains approximately constant to within the error of the measurement. The second observation is a kink in the temperature profile coinciding with the upper edge of the dark layer. The jump in the temperature gradient associated with this kink is not attributable to the release of latent heat from the formation of ice because it occurs well above the freezing point. Rather, it signals an abrupt change in the particle concentration, revealing the location of a sharp compaction front at the boundary between the dark layer and the bulk suspension.

The claim that this boundary is a compaction front is easily verified by applying a heat balance at the point of the jump in temperature gradient, which gives

$$\left(k_e \frac{dT}{dz}\right)_+ = \left(k_e \frac{dT}{dz}\right)_- \quad (1)$$

where k_e is the effective thermal conductivity of the suspension and the subscripts + and − refer to quantities on the top and bottom sides, respectively, of the compaction front. The large difference in the thermal conductivities of alumina and liquid water, $k_p = 35$ W m^{-1} K^{-1} and $k_l = 0.6$ W m^{-1} K^{-1}, respectively, leads to an effective thermal conductivity that is sensitive to particle concentration, and for the present case where $k_p > k_l$, the value of k_e increases monotonically with particle concentration.[38] From eq 1, it follows that, at the compaction front, where $(k_e)_+ < (k_e)_-$, it must be the case that $(dT/dz)_+ > (dT/dz)_-$. This is consistent with the temperature gradient shown in Figure 5, which was computed from a continuous piecewise polynomial fit of the temperature profile.

The accumulation of particles in the dark layer is the result of particle rejection by the ice lenses at low freezing rates. Peppin et al.[4] presented a mathematical model describing this situation for a hard-sphere colloidal suspension and showed that the boundary layer of rejected particles becomes separated from the bulk suspension by a sharp compaction front as the particles in the layer become close-packed. More generally, colloidal dispersions are observed to accumulate readily into uniform, close-packed layers in many processes where there is removal of the liquid phase from the boundary, such as in drying,[30,32,39] filtration,[40] and ceramics casting.[41] The length scale over which the particle concentration varies across the compaction front is given by the diffusional length scale, $l_D = D_0/V$, where $D_0 = k_B T/6\pi R\mu$ is the Stokes−Einstein diffusivity, $k_B T$ is the thermal energy for Brownian motion, R is the particle radius, and μ is the viscosity of water. For 0.3-μm particles and a freezing rate of $V = 1$ μm s^{-1}, this gives $l_D \approx 1$ μm, which predicts a very sharp transition in particle concentration, consistent with our observations. This general picture for the formation of the compaction front should remain valid for the charged alumina particles used here, as a hard-sphere model gives a reasonable approximation over a large range of particle concentrations when the electric double layers surrounding the particles are thin[42] (here, $\kappa R \approx 10$, where the Debye length κ^{-1} gives the thickness of the double layers). However, a hard-sphere description begins to falter near close-packing, when the electric double layers overlap, and a closer examination of the particle interactions in the dark layer is necessary.

For instance, when a compacted layer forms during the freezing of a hard-sphere colloidal suspension, it will disperse under the Brownian motion of the particles when freezing is

dx.doi.org/10.1021/la303458m | Langmuir 2012, 28, 16512−16523

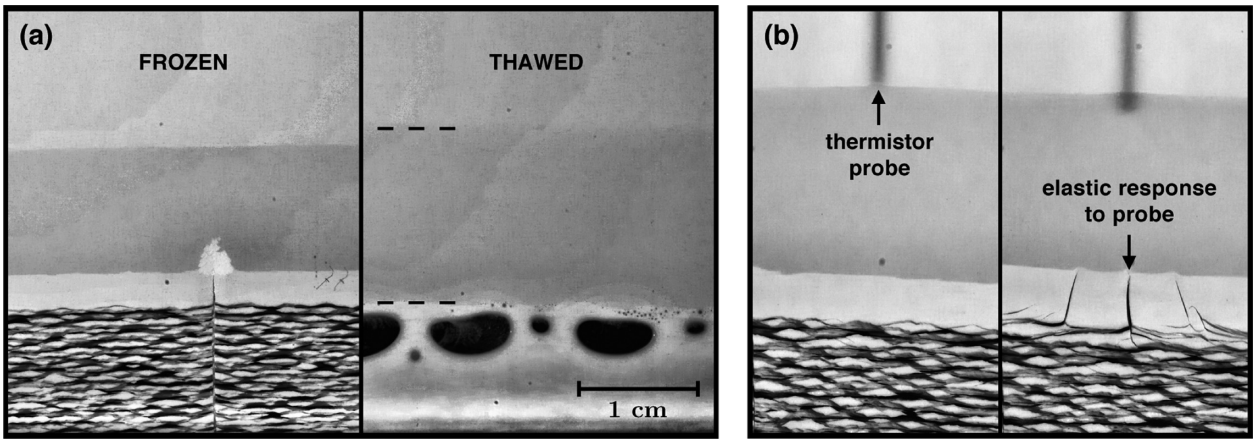

Figure 6. (a) Frozen sample (left) in steady state at a freezing rate of 1 μm/s and (right) 60 min after it had completely thawed. The compacted layer, extending to the top of dark layer, does not redisperse during remelting. As the segregated ice melted, water rose and collected in pockets underneath the aggregated layer. These pockets of water might be the origin of the potholes in our roads after a spring thaw. (b) As the thermistor probe made contact with the dark layer, cracks instantaneously appeared at the base of the layer, demonstrating the elastic nature of the aggregated layer (see also Movie S5, Supporting Information).

halted and the suspension is allowed to remelt. When this test was performed on the frozen alumina suspensions, the compacted layer did not disperse but remained intact as a cohesive aggregated layer. Figure 6a shows side-by-side images of a sample taken during steady-state freezing at $V = 1$ μm s^{-1} and 1 h after the sample had completely remelted, which took approximately 20 min once the coolers had been turned off. The aggregated suspension trapped between ice lenses sedimented to the bottom of the cell as the meltwater ascended and accumulated in visible pockets underneath the rigid and relatively impermeable dark layer in the thawed sample.

There was some thickening of the dark layer in the thawed sample. We believe that this can be attributed to elastic relaxation once the large compressive forces exerted on the aggregated layer by the segregated ice growth were relieved upon melting. A further demonstration that the dark layer compacted into an elastic state is given in Figure 6b, where the frozen sample is shown immediately before and after the thermistor probe came into contact with the dark layer. Once contact had been made, stress was transmitted almost instantaneously through the layer, causing further ice segregation in the vicinity of the ice lenses. The rapid response of the system to elastic stress is more evident from Movie S5 (Supporting Information).

The stress associated with segregated ice growth, which puts the liquid into tension and consolidates the particles, is referred to as cryosuction. For aggregation to occur, cryosuction must transmit sufficiently large compressive forces onto the particles to overcome their electrostatic repulsions, thereby forcing the particles into contact, where they remain cohesively bound by van der Waals attractions.[28] Such a stress-induced sol−gel transition is irreversible, which explains the persistence of the dark layer in the thawed samples. The forced aggregation of electrostatically stabilized dispersions into a dense cohesive layer has been observed in centrifuge experiments[28,29] and in directional drying experiments,[31,32,37] where capillary stresses play role analogous to that of cryosuction. In the next section, cryosuction is quantified, and a simple freezing model is presented to assess the role of cryosuction in producing particle aggregation ahead of a growing sequence of ice lenses.

We conclude this section with observations about the light-colored layer located immediately ahead of the warmest ice lens that are pertinent to our model of the freezing behavior. Note that the light-colored layer vanished upon melting in Figure 6a and that the region it occupied became indistinguishable from the rest of the aggregated layer. This could be an indication that the light-colored region contained ice. This possibility is reinforced by the temperature measurements (Figure 5), which establish that the entirety of the light-colored layer existed below the bulk freezing point. Although the refractive indices of the solid and liquid phases of water are similar, 1.31 and 1.33, respectively, the reflective nature of finely grained ice can render such ice optically distinguishable from liquid water. For example, this optical effect is present in the eutectic phases of aqueous salt solutions, whose white color is a result of polycrystalline ice. (For example, see Figure 3 in Peppin et al.,[43] showing an aqueous NH_4Cl eutectic phase in the same directional solidification apparatus as used here.) When a frozen fringe is present, such that ice is interspersed within the pore space of the particle matrix, the sample is expected to be highly polycrystalline,[44] much like a eutectic phase. We therefore speculate that the light-colored layer is a frozen fringe, and in the next section, we provide quantitative measurements that are broadly consistent with this hypothesis.

It is also instructive to examine the transient development of the light-colored layer (see Movie S6, Supporting Information). During the evolution toward a steady state, the light-colored region is initiated at several points in the aggregated suspension at the top of a segregated layer of ice. These points of origin spread laterally and merge into a continuous layer that advances ahead of the segregated ice. The formation of the light-colored layer always precedes the formation of ice lenses. We note this because, in some theories of frost heave, a frozen fringe is required to produce ice lenses.[20−22] As the leading edge of the light layer moves forward, it advances in discrete steps as new points extend from the leading edge and quickly spread laterally. This stepwise advance of the light-colored layer could be the result of a surface energy barrier that must be overcome before ice can pass through narrow pore spaces. Alternatively, it could be a consequence of the intermittent formation of the ice lens and the associated jumps in cryosuction pressure.

dx.doi.org/10.1021/la303458m | *Langmuir* 2012, 28, 16512−16523

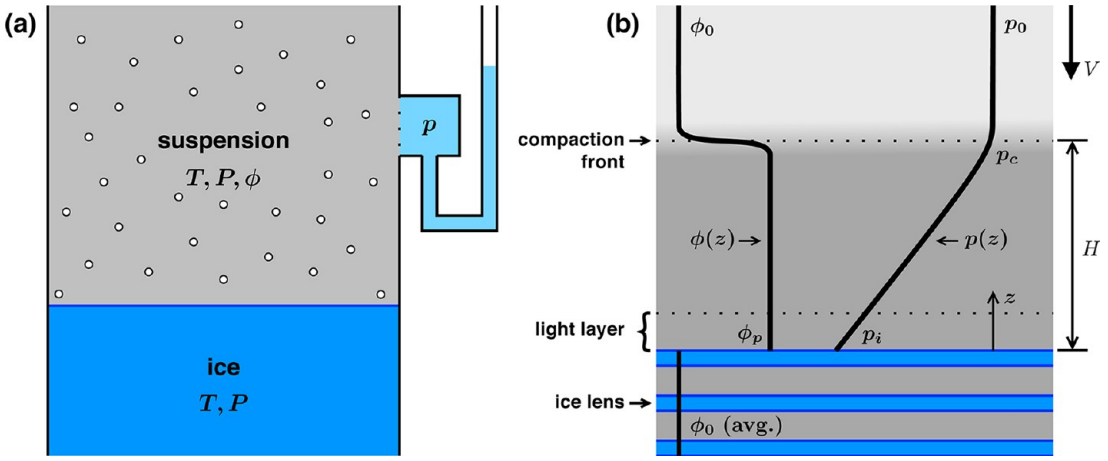

Figure 7. (a) Thermodynamic configuration of an ice-suspension system held at fixed temperature T and external pressure P. The suspension has a particle fraction ϕ, and all particles were excluded from the ice. Water was allowed to pass through a rigid, semipermeable membrane into a reservoir in equilibrium with the suspension. The pressure p measured in the reservoir defines the pervadic pressure of the suspension. (b) Diagram showing the vertical structure of the aggregated layer formed ahead of a sequence of ice lenses growing at speed V.

Finally, we comment on the appearance of the particle-rich layers that develop between ice bands at high freezing rates (Figure 3g–i). Upon close inspection of the particle-rich layers (inset of Figure 3i), there appears to be further segregation of ice at the submillimeter scale. The possibility of segregated ice in the particle layers at high freezing rates is consistent with the experiments of Deville et al.,[5] which identified vertical dendritic ice crystals in the particle-rich layers separated by intermittent particle-free ice bands. Moreover, when an appreciable portion of ice becomes segregated from the suspension, rather than interspersed in the pore space, this might significantly reduce the polycrystallinity in that region. According to the remarks made above, the formation of dendritic ice might also explain the lack of a detectable color change in the particle-rich layers even as the temperature drops well below the bulk freezing point near the cold heat-exchanger plate.

Particle Aggregation: A Simple Model. When a macroscopic region of segregated ice is cooled below the bulk freezing temperature $T_m = 0$ °C, the liquid in the adjacent suspension is brought into tension, producing the effect known as cryosuction. The Clausius–Clapeyron equation,

$$P - p = \mathcal{L}(T_m - T) \tag{2}$$

provides an equilibrium relationship between the temperature T of the segregated ice and the "pervadic pressure"[45] p of the liquid in the suspension at a fixed external pressure P, where $\mathcal{L} = \rho_l q_m / T_m$ is the Clausius–Clapeyron slope, ρ_l is the liquid density, and q_m is the specific heat of fusion. For an ice-suspension system, $\mathcal{L} = 1.2$ MPa K^{-1}. As shown in Figure 7a, the pervadic pressure is defined as the pressure in a reservoir of liquid separated from the suspension by a rigid membrane that is permeable to water but not to particles. Peppin et al.[45] showed this to be a convenient choice for analyzing the consolidation of a suspension because the definition of p is independent of any details about the suspension, such as whether it is dispersed or aggregated into a rigid porous layer. In both of these examples, there is a familiar physical meaning attached to p: In the case of an aggregated layer, p is the Darcy pressure measured in porous media flow; in the case of a dispersion, p is related to the osmotic pressure Π of the dispersion, by $\Pi = P - p$,[45] which originates in part from the Brownian motion of the colloidal particles and can be thought of as the effective interparticle pressure.

Referring to the temperature profile in Figure 5 and using eq 2, the temperature measured at the warmest ice lens $T_i \approx -2$ °C implies a pressure drop $(P - p_i)$ of over 2 MPa in the adjacent suspension. This pressure drop drives fluid flow toward the ice lens to enable its growth while maintaining a concentrated boundary layer of particles. To predict the state of the concentrated particle layer, that is whether it is aggregated, it is necessary to quantify the extent to which the particle interactions can resist consolidation. In general, the osmotic pressure of a dispersion increases (reversibly) with particle concentration up to a critical value Π_c, beyond which the dispersion becomes irreversibly aggregated. For electrostatically stabilized dispersions, the value of Π_c has been found to be well correlated with the DLVO (Deryagin–Landau–Verwey–Overbeek) pair potential.[29] Based on values reported for latex lattices with DLVO characteristics similar to those of the alumina suspensions used here, $\Pi_c \approx 10$ kPa provides an approximate upper bound.[28,29,32] Because this critical value is much smaller than the stresses arising from cryosuction, an appreciable aggregated layer can form.

A prediction for the steady-state thickness H of the aggregated layer requires an appropriate model for the flow induced by ice-lens formation. The scenario as it pertains to our experiments is illustrated in Figure 7b, which shows the structure of the suspension ahead of a series of ice lenses growing at speed V. Darcy's equation, given by

$$\mu u = -k(\phi)\nabla p \tag{3}$$

relates gradients in p to the volume flux u of water through the porous layer supplying ice-lens growth, where μ is the liquid viscosity and $k(\phi)$ is the permeability, which is a function of particle volume fraction ϕ. In steady state, volume balances for liquid and particles at the compaction front give

$$v_l = -V\left(\frac{1-\phi_0}{1-\phi}\right) \quad \text{and} \quad v_p = -V\left(\frac{\phi_0}{\phi}\right) \tag{4}$$

where v_l and v_p are the volume-averaged liquid and particle velocities, respectively, and ϕ_0 is the particle concentration of the bulk suspension. Combining these expressions gives

dx.doi.org/10.1021/la303458m | Langmuir 2012, 28, 16512–16523

$$u \equiv (1 - \phi)(v_l - v_p) = -V\left(\frac{\phi - \phi_0}{\phi}\right) \quad (5)$$

Assuming that the aggregated layer is both uniformly close-packed and uniformly permeable, eqs 3 and 5 combine to give a constant pressure gradient across the layer, given by

$$\nabla p = \frac{p_c - p_i}{H} = \frac{\mu(\phi - \phi_0)V}{\phi k(\phi)} \quad (6)$$

where p_i is the value at $z = 0$ obtained from eq 2 and $p_c = P - \Pi_c$ is the critical value of the pervadic pressure attained at the leading edge of the aggregated layer $z = H$.

For the pulling speed $V = 1\ \mu\text{m s}^{-1}$, where the measured thickness of the aggregated layer is $H \approx 12$ mm (taking the combined thickness of the dark and light layers in Figure 5), the pressure drop across the layer given by eq 6 is predicted to be

$$p_c - p_i = (1.6 \times 10^{13}\ \text{Pa s m}^{-2})HV \approx 0.2\ \text{MPa} \quad (7)$$

computed using $\phi_0 = 0.27$ for the bulk concentration, $\phi \approx 0.64$ for a randomly close-packed layer, $\mu = 1.8 \times 10^{-3}$ Pa s for the viscosity of water, and the Kozeny–Carmen equation $k = R^2(1 - \phi)^3/45\phi^2 = 6.5 \times 10^{-17}$ m^2 to estimate the permeability of the layer for particles with radius $R = 0.16\ \mu$m. Comparing this result with the pressure drop inferred from eq 2,

$$p_c - p_i = (1.2\ \text{MPa K}^{-1})(T_m - T_i) - \Pi_c \approx 2.6\ \text{MPa} \quad (8)$$

computed using the bulk freezing temperature $T_m = 0$ °C and the measured ice-lens temperature $T_i = -2.2$ °C, there is a difference of more than an order of magnitude between the two predictions.

Further considerations might explain the discrepancy between eqs 7 and 8. The first is due to the presence of free ions in the suspension, which can build up in front of an ice lens and depress the freezing point T_m, thereby reducing the effective undercooling $T_m - T_i$ and the magnitude of the cryosuction at the warmest ice lens. The second consideration is due to the presence of a thin premelted film maintained by the disjoining pressure between the ice and particle phases. Flow in this premelted film, which is necessary for ice growth, leads to an additional viscous pressure drop at the ice–suspension interface. Other studies have shown that this "contact resistance" can become important at sufficiently high freezing rates.[46,47] A third possibility is the existence of a frozen fringe, as described above, which could also serve to decrease the permeability near the ice lens appreciably and therefore enhance the dissipation of the cryosuction pressure. Each of these possibilities is appraised in more detail below.

For dilute solute concentrations C, the freezing point depression follows a linear relationship, $T_m^* = T_m + mC$, where $m < 0$ is the slope of the liquidus curve in the binary phase diagram. Free ions in the alumina suspensions are expected to come primarily from the addition of HCl. The liquidus slope of dilute aqueous HCl solutions has the value $m = -1.2$ °C/(wt %). Because the suspensions used here were prepared at pH 5, we assume the bulk concentration of HCl to be $C_0 = [H^+] = 10^{-5}$ M (3.7×10^{-5} wt %). Solute, like colloid, is almost completely rejected by ice, such that, with the formation of each new ice lens, a solutal boundary layer will accumulate until the next ice lens emerges, trapping some portion of the rejected solute between them, and then the process repeats. In steady state, the time-averaged concentration of solute at the warmest ice lens C_i can be estimated from a mass balance $C_0 = k_s C_i$, where k_s is a segregation coefficient that depends on the relative thicknesses of the solute-free ice lenses λ_i and the intervening particle layer λ_s, according to $k_s \approx \lambda_s/(\lambda_s + \lambda_i)$. In the experiments, we observed that λ_s was approximately equal to λ_i, giving $k_s \approx 0.5$. According to these estimates, $C_i \approx C_0$, which leads to an estimated adjustment of $T_m - T_m^* \approx 4 \times 10^{-5}$ °C to the freezing point at the active ice lens, nowhere near the approximately 2 °C needed to reconcile eqs 7 and 8.

The importance of contact resistance at the ice–suspension interface can be assessed from theoretical arguments offered by Style and Peppin,[47] who compared the viscous resistance at the interface, $f_i \approx \mu R^2/d^3$, where R is the mean particle radius and $d = d(T)$ is the temperature-dependent thickness of the premelted film, to the resistance of the porous aggregated layer, $f_p = \mu H/k$, which follows from eq 3. A ratio of $f_i/f_p \approx R^2k/Hd^3 \gtrsim O(1)$ requires a film thickness of $d \lesssim 1$ nm. We are not aware of any study that directly measures $d(T)$ for charged alumina surfaces; however, Hansen-Goos and Wettlaufer[48] provided a detailed theoretical description of the dependence of the premelted film thickness on undercooling and showed that ions in solution generally lead to thicker premelted films due to electrostatic repulsions, which tend to dominate van der Waals forces in the range of undercooling of interest here. For the value of undercooling $\Delta T \approx 2$ °C measured at the ice lens, $d \approx 10$ nm is predicted,[48] giving $f_i/f_p \approx 10^{-3}$. This suggests that contact resistance is secondary to the viscous resistance in the aggregated layer. Finally, even for $f_i \approx f_p$, we still cannot account for the fact that the total viscous resistance, $P_c - P_i \approx V(f_i + f_p)$, is approximately 1 order of a magnitude smaller than given by eq 8. If contact resistance were to account for the required pressure drop, the premelted film would need a thickness of $d \approx 1$ Å.

A frozen fringe can form provided that the suspension is sufficiently undercooled, a consequence of the curvature-induced depression of the freezing point for water occupying a submicrometer-sized pore. The temperature T_f at which a grain of ice with curvature $\mathcal{K} = 2/R_i$ can form is given by the Gibbs–Thomson equation

$$\frac{2}{R_i} = \left(\frac{\rho_s q_m}{\gamma_{sl}}\right)\frac{T_m - T_f}{T_m} \quad (9)$$

where $\rho_s = 0.917$ g cm^{-3} is the density of ice and $\gamma_{sl} = 2.9 \times 10^{-2}$ J m^{-2} is the surface energy of ice in contact with liquid water. If R_p is the characteristic pore radius of a particle matrix, then pore ice can exist at temperatures where $R_i \le R_p$. For randomly close-packed spheres, there is a distribution of pore sizes, leading to uncertainty in the value of R_p. Moreover, from simulated close packings, Nolan and Kavanagh[49] showed that the pore-size distribution is broadened by increasing polydispersity in particle size. The alumina particles used in the present study closely follow a log-normal size distribution with a 20% variance. For the same particle distribution, with mean particle radius $\langle R \rangle$, the pore radii are predicted to be as large as $R_p^u \approx 0.6\ \langle R \rangle$, beyond which the probability for larger pores is substantially diminished.[49] Nolan and Kavanagh also determined the size range of spheres that could successfully percolate through a close-packed matrix and found a maximum percolation radius of approximately $R_p^l \approx 0.2\langle R \rangle$ for the same degree of polydispersity. From these pore-size metrics, R_p^u and R_p^l, we estimate a range of

dx.doi.org/10.1021/la303458m | Langmuir 2012, 28, 16512–16523

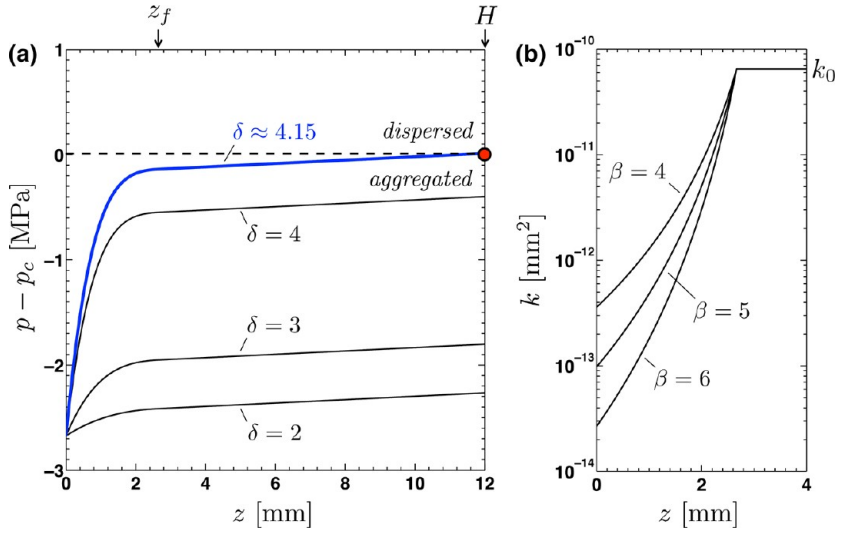

Figure 8. Results of a flow model including a frozen fringe. (a) Plots of the pressure obtained from Darcy's equation (eq 11) for various values of $\delta = \beta - \alpha$ ($V = 1$ μm s^{-1}, $T_i = -2.2$ °C, $T_f = -0.6$ °C, $G = 0.6$ °C mm^{-1}, $\phi_0 = 0.27$, $\phi = 0.64$, $k_0 = 6.5 \times 10^{-11}$ mm^2, $\mu = 1.8 \times 10^{-3}$ Pa s, $\Pi_c = 10$ kPa). The frozen fringe lies in the range $0 \le z \le z_f$. For the value $\delta \approx 4.15$, the pressure attains a critical value p_c (dashed line) at $z \approx 12$ mm, the position at the top of the aggregated layer measured experimentally. (b) Plots of the permeability for different values of β. Outside the frozen fringe, the permeability takes a constant value k_0.

possible ice-entry temperatures, -1.6 °C $\lesssim T_f \lesssim -0.5$ °C. Note that the isotherm along the top edge of the light-colored layer, measured to be approximately -0.6 °C, is in closer agreement with the upper bound (see Figure 5). This might be an indication of heterogeneous ice nucleation on the particle surfaces or of incomplete premelting[50] allowing ice to advance through the pores with contact angles less than 180°. In the next section, we modify the simple freezing model used in this section to allow for pore ice in the light-colored layer.

Frozen Fringe. To include a frozen fringe in the freezing model, modifications must account for the fact that, as the temperature is reduced below ice-entry temperature T_f, the fraction of ice occupying the pore space continues to increase and a diminishing fraction of liquid remains in the regions of high curvature (e.g., near particle contacts) and in thin premelted liquid films at the surfaces of the particles.[44,48] A continuous liquid network is therefore maintained within the frozen fringe, which has a shrinking permeability with decreasing temperature.

Models[22,44,48] for the fraction of ice occupying the pore space f_i and the permeability k_f are given by relationships of the form

$$f_i(T) = 1 - \left(\frac{T_m - T_f}{T_m - T}\right)^{\alpha} \quad \text{and} \quad k_f = k_0(1 - f_i)^{\beta/\alpha} \tag{10}$$

for $T \le T_f$, reflecting the continuous nature of the phase transformation in porous media. Here, k_0 is the permeability of the unfrozen aggregated layer, and the exponents α and β depend on microphysical details of the ice–liquid equilibrium.[44,48] Taking into account the portion of the water that is converted to pore ice, the volume flux of liquid within the frozen fringe is given by $u_f = (1 - f_i)u$, where u is the flow rate in the unfrozen layer from eq 5. Using Darcy's equation (eq 3) with eq 10, it follows that

$$\frac{dp}{dz} = \frac{\mu V}{k_0}\frac{\phi - \phi_0}{\phi}\left(\frac{T_m - T_f}{T_m - T}\right)^{-\delta} \tag{11}$$

for $T \le T_f$, where $\delta \equiv \beta - \alpha$. To demonstrate the impact of the frozen fringe, solutions to eq 11 were obtained for a linear temperature field $T = T_i + Gz$, with gradient G. These solutions are shown in Figure 8 for different values of δ over the interval between the warmest ice lens and the top of the aggregated layer (parameter values are given in the figure caption). For $\delta \approx 4.15$, the entire pressure drop generated by cryosuction can be explained, with nearly 90% of the total pressure drop occurring within the frozen fringe. There is a small sample of experiments on naturally occurring clays and silts showing a large variability in the values of α and β.[51] For the range of undercooling considered here, the theoretical model of Cahn et al.[44] suggests $\alpha = 2$, assuming that the majority of the premelted liquid is located in pendular rings near particle contacts.[22] With this choice, our experiments predict a value of $\beta \approx 6.15$ for the permeability exponent.

Ice-Lens Statistics. The experimental images for low freezing rates were analyzed to compile statistics on the following characteristics of the steady-state ice segregation patterns: ice-lens thickness (λ_i), separation (λ_s), and total spacing ($\lambda = \lambda_i + \lambda_s$). Once a steady state had been achieved for a given pulling speed, freezing was continued over several generations of ice lenses, and the acquired images were assembled into a single image containing a long sequence of ice lenses. The compiled image was then thresholded to distinguish segregated ice from particles and facilitate their measurement (Figure 9a). Finally, the values for λ, λ_i, and λ_s were computed along several vertical slices in each thresholded image. The value of λ was found to be insensitive to the threshold level, whereas those of λ_i and λ_s were not. To estimate λ_i and λ_s, we chose to constrain the thresholding limit in order to conserve the volume of particles in steady state. This was accomplished by computing the area of the white (A_w) and black (A_b) regions in the binary image and choosing the thresholding limit to satisfy the constraint $\phi_p A_w = \phi_0(A_w + A_b)$, which equates the volume of particles in the white regions with the volume of particles supplied by the bulk suspension. The results are shown in Figure 9b for several pulling speeds. These ice-lens

dx.doi.org/10.1021/la303458m | Langmuir 2012, 28, 16512–16523

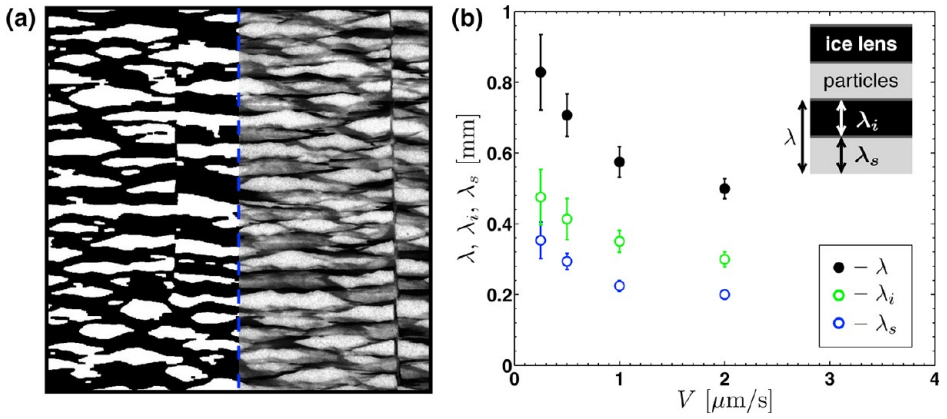

Figure 9. (a) Image showing several generations of ice lenses at $V = 1$ μm s^{-1}. The left half of the image shows the result of thresholding to separate ice lenses (black) from the intermediate particle layers (white), enabling a statistical analysis of the pattern. (b) Plots of the ice-lens thickness (λ_i), separation (λ_s), and total spacing ($\lambda = \lambda_i + \lambda_s$) compiled from the thresholded images as a function of the pulling speed. Each of these quantities was found to decrease with increasing V.

statistics confirm that the mean length scale decreases with increasing pulling speed.

DISCUSSION

In this article, two distinct modes of periodic ice banding have been illustrated in steady-state directional solidification experiments with electrostatically stabilized alumina dispersions. At low freezing rates (0.25−3 μm s^{-1}), the pattern of ice segregation was remarkably cracklike and accompanied by additional structure in the suspension, formed by a layer of particles rejected from a regular sequence of ice lenses. At higher freezing rates (5−10 μm s^{-1}), intermittent ice bands, which do not resemble cracks, emerged from a suspension that is absent of any visible structure. To gain further insight into the physical processes leading to ice segregation in these two regimes, a detailed investigation of the boundary layer of rejected particles was conducted. In this section, we summarize the key experimental observations and highlight areas for further study.

The freezing behavior at low pulling speeds shares some common features with drying fronts observed in colloidal dispersions. Although there are important differences between cryosuction generated by segregated ice and capillary pressure from fluid menisci at the evaporating edge of a drying suspension, both forces serve to remove liquid from the suspension, resulting in the accumulation of particles into a close-packed porous layer. When ice lenses were present, we showed that the compressive stresses from cryosuction exceeded the critical aggregation pressure of the alumina dispersions by several orders of magnitude, resulting in the formation of a cohesive porous layer of appreciable thickness that is easily discernible as a dark-colored region in the experimental images (Figure 3a−c). The dark aggregated layer is separated from the bulk suspension at a sharp compaction front, due to the small diffusional length scale of the alumina particles. Irreversible particle aggregation has been shown to be a salient feature in drying phenomena.[30,32,34,37] Based on typical aggregation pressures for electrostatically stabilized dispersions, our observations suggest that particle aggregation might be an unavoidable feature when ice segregation occurs in these systems.

A light-colored layer appears in the freezing images at low freezing rates when the temperature in the aggregated layer falls below the bulk freezing point. We propose that this color change arises from specular reflections from grains of pore ice, signaling the presence of a frozen fringe. Further experiments are required to determine conclusively whether pore ice is present in this layer. However, our estimates suggest that the existence of pore ice, which significantly reduces the permeability of the medium, is the only plausible explanation for the large cryosuction forces associated with the undercooling of the warmest ice lens.

A frozen fringe has important theoretical implications for the prediction of ice-lens formation. Disjoining forces within the frozen fringe generate a thermomolecular pressure gradient, which acts to push the particles along the temperature gradient toward warmer temperatures.[22] The particle matrix can therefore be brought into tension at a location where the thermomolecular force overcomes the hydrodynamic drag set up by the flow of liquid feeding ice lens growth. One of the central ideas of rigid-ice models[20−22] is that a new ice lens emerges within the frozen fringe where the tension first exceeds the cohesive strength of the particle matrix. Recently, Style et al.[25] proposed a model for ice-lens growth in a cohesive medium through the extension of horizontal ice-filled cracks that might not need a frozen fringe but would then need significant gradients of solute. In Movie S4 (Supporting Information), we see what appears to be the horizontal extension of cracks as new ice lenses are initiated, which could support the picture assumed by Style et al. but could also be consistent with the rigid-ice mechanism as a nucleation criterion. In light of our experimental findings, there appears to be a need to reconcile these two theories in order to clarify the mechanism of ice-lens formation.

The directional freezing experiments used here have a number of advantages for testing models of ice segregation. One advantage is that the freezing apparatus allows independent control of the freezing rate and temperature gradient, thus providing a steady state that is amenable to mathematical analysis. A long-standing difficulty of comparing models with previous experimental measurements is the need to specify the location of a hydrostatic reservoir, where the water is drawn from to supply ice-lens growth. The location of this reservoir is typically unknown, or when it is known, the position is not fixed relative to the position of the freezing front. This ambiguity is overcome in the present experiments

dx.doi.org/10.1021/la303458m | Langmuir 2012, 28, 16512−16523

because the reservoir is simply located at the top edge of the aggregated layer, which is determined dynamically as part of the steady state and is readily detectable in the freezing suspensions.

Finally, we conclude with a few remarks about the ice banding at high freezing rates. A transition to this mode of banding occurs once the dark-colored layer becomes significantly diminished, around $V = 4\ \mu\text{m s}^{-1}$. Because a cohesive layer can resist deformation, it is possible that the aggregated particles suppress morphological instabilities.[23,24] At high freezing rates, where the cohesive layer is thinner or absent, the ice lenses below might become prone to morphological instability. Indeed, this separate mode of ice banding appears to be similar to that observed by Deville et al.[5] in freezing experiments with alumina suspensions, where the particle-rich layers between ice bands were found to contain vertically aligned dendritic ice crystals. Noting that disequilibrium could play a factor at higher freezing rates, Elliott and Peppin[27] suggested particle capture to explain this mode of banding, in a manner completely analogous to solute banding in rapid alloy solidification. The steady-state experiments presented in this article could prove to be fertile testing grounds for these theories as well.

■ ASSOCIATED CONTENT

Supporting Information

Supporting movies, along with a short description of each movie. This material is available free of charge via the Internet at http://pubs.acs.org.

■ AUTHOR INFORMATION

Corresponding Author

*E-mail: aa644@cam.ac.uk.

Notes

The authors declare no competing financial interest.

■ ACKNOWLEDGMENTS

This work has benefitted greatly from countless discussions with Drs. Stephen Peppin and Robert Style. The authors also thank Prof. John Wettlaufer for his scientific insights and David Page-Croft, in the George Batchelor Laboratory at DAMTP, for his patient technical support. This material is based on work supported by the National Science Foundation under Award OISE-0965138 (AMA).

■ REFERENCES

(1) Taber, S. Frost heaving. *J. Geol.* **1929**, *37*, 428.
(2) Taber, S. The mechanics of frost heaving. *J. Geol.* **1930**, *38*, 303.
(3) Deville, S.; Saiz, E.; Nalla, R. K.; Tomsia, A. P. Freezing as a path to build complex composites. *Science* **2006**, *311*, 515.
(4) Peppin, S. S. L.; Elliott, J. A. W.; Worster, M. G. Solidification of colloidal suspensions. *J. Fluid Mech.* **2006**, *554*, 147.
(5) Deville, S.; Maire, E.; Bernard-Granger, G.; Lasalle, A.; Bogner, A.; Gauthier, C.; Leloup, J.; Guizard, C. Metastable and unstable cellular solidification of colloidal suspensions. *Nat. Mater.* **2009**, *8*, 966.
(6) Zhang, H.; Hussain, I.; Brust, M.; Butler, M. F.; Rannard, S. P.; Cooper, A. I. Aligned twoand three-dimensional structures by directional freezing of polymers and nanoparticles. *Nat. Mater.* **2005**, *4*, 787.
(7) Deville, S.; Saiz, E.; Tomsia, A. P. Ice-templated porous alumina structures. *Acta Mater.* **2007**, *55*, 1965.
(8) Rapatz, G.; Menz, L. J.; Luyet, B. J. In *Cryobiology*; Meryman, H. T., Ed.; Academic Press: New York, 1966; pp 139−162.
(9) Mazur, P. Freezing of living cells: Mechanisms and implications. *Am. J. Physiol. Cell Physiol.* **1984**, *247*, 125.
(10) Velez-Ruiz, J. F.; Rahman, M. S. In *Handbook of Food Preservation*, 2nd ed.; Rahman, M. S., Ed.; CRC Press: Boca Raton, FL, 2007; Chapter 26, p 635.
(11) Gay, G.; Azouni, M. A. Forced migration of nonsoluble and soluble metallic pollutants ahead of a liquid−solid interface during unidirectional freezing of dilute clayey suspensions. *Cryst. Growth Des.* **2002**, *2*, 135.
(12) French, H. M. *The Periglacial Environment*; John Wiley and Sons: New York, 2007.
(13) Matsuoka, N.; Murton, J. Frost weathering: Recent advances and future directions. *Permafrost Periglac.* **2008**, *19*, 195.
(14) Uhlmann, D. R.; Chalmers, B.; Jackson, K. A. Interaction between particles and a solid/liquid interface. *J. Appl. Phys.* **1964**, *35*, 2986.
(15) Chernov, A. A.; Temkin, D. E.; Mel'nikova, A. M. Theory of the capture of solid inclusions during the growth of crystals from the melt. *Sov. Phys. Crystallogr.* **1976**, *21*, 369.
(16) Rempel, A. W.; Worster, M. G. The interaction between a particle and an advancing solidification front. *J. Cryst. Growth* **1999**, *205*, 427.
(17) Wettlaufer, J. S.; Worster, M. G. Premelting dynamics. *Annu. Rev. Fluid Mech.* **2006**, *38*, 427.
(18) Mutou, Y.; Watanabe, K.; Ishikazi, T.; Mizoguchi, M. In *Proceedings of the 7th International Conference on Permafrost, Yellowknife, Canada*; Laval University: Quebec, Canada, 1998; p 783.
(19) Watanabe, K.; Mizoguchi, M. Ice configuration near a growing ice lens in a freezing porous medium consisting of micro glass particles. *J. Cryst. Growth* **2000**, *213*, 135.
(20) O'Neill, K.; Miller, R. Exploration of a rigid-ice model of frost heave. *Water Resour. Res.* **1985**, *21*, 281.
(21) Fowler, A. C. Secondary frost heave in freezing soils. *SIAM J. Appl. Math.* **1989**, *49*, 991.
(22) Rempel, A. W.; Wettlaufer, J. S.; Worster, M. G. Premelting dynamics in a continuum model of frost heave. *J. Fluid Mech.* **2004**, *498*, 227.
(23) Peppin, S. S. L.; Worster, M. G.; Wettlaufer, J. S. Morphological instability in freezing colloidal suspensions. *Proc. R. Soc. A* **2007**, *463*, 723.
(24) Peppin, S. S. L.; Wettlaufer, J. S.; Worster, M. G. Experimental verification of morphological instability in freezing aqueous colloidal suspensions. *Phys. Rev. Lett.* **2008**, *100*, 238301.
(25) Style, R. W.; Peppin, S. S. L.; Cocks, A. C. F.; Wettlaufer, J. S. Ice-lens formation and geometrical supercooling in soils and other colloidal materials. *Phys. Rev. E* **2011**, *84*, 041402.
(26) Lasalle, A.; Guizard, C.; Maire, E.; Adrien, J.; Deville, S. Particle redistribution and structural defect development during ice templating. *Acta Mater.* **2012**, *60*, 4594−4603.
(27) Elliott, J. A. W.; Peppin, S. S. L. Particle trapping and banding in rapid colloidal solidification. *Phys. Rev. Lett.* **2011**, *107*, 168301.
(28) Meijer, A. E. J.; van Megen, W. J.; Lyklema, J. Pressure-induced coagulation of polysyrene latices. *J. Colloid Interface Sci.* **1978**, *66*, 99.
(29) Bensley, C. N.; Hunter, R. J. The coagulation of concentrated colloidal dispersions at low electrolyte concentrations: II. Experimental coagulation pressures. *J. Colloid Interface Sci.* **1983**, *92*, 448.
(30) Tsapis, N.; Dufresne, E. R.; Sinha, S. S.; Riera, C. S.; Hutchinson, J. W.; Mahadevan, L.; Weitz, D. A. Onset of buckling in drying droplets of colloidal suspensions. *Phys. Rev. Lett.* **2005**, *94*, 018302.
(31) Dufresne, E. R.; Stark, D. J.; Greenblatt, N. A.; Cheng, J. X.; Hutchinson, J. W.; Mahadevan, L.; Weitz, D. A. Dynamics of fracture in drying suspensions. *Langmuir* **2006**, *22*, 7144.
(32) Goehring, L.; Clegg, W. J.; Routh, A. F. Solidification and ordering during directional drying of a colloidal dispersion. *Langmuir* **2010**, *26*, 9269.
(33) Scales, P. J.; Johnson, S. B.; Healy, T. W.; Kapur, P. C. Shear yield stress of partially flocculated colloidal suspensions. *AIChE J.* **1998**, *44*, 538.

(34) Chiu, R. C.; Garino, T. J.; Cima, M. J. Drying of granular ceramic films: I, Effect of processing variables on cracking behavior. *J. Am. Ceram. Soc.* **1993**, *76*, 2257.
(35) Chamberlain, E. J.; Gow, A. J. Effect of freezing and thawing on the permeability and structure of soils. *Eng. Geol.* **1979**, *13*, 73−92.
(36) Allain, C.; Limat, L. Regular patterns of cracks formed by directional drying of a colloidal suspension. *Phys. Rev. Lett.* **1995**, *74*, 2981.
(37) Dufresne, E. R.; Corwin, E. I.; Greenblatt, N. A.; Ashmore, J.; Wang, D. Y.; Dinsmore, A. D.; Cheng, J. X.; Xie, X. S.; Hutchinson, J. W.; Weitz, D. A. Flow and fracture in drying nanoparticle suspensions. *Phys. Rev. Lett.* **2003**, *91*, 224501.
(38) Batchelor, G. K. Transport properties of two-phase materials with random structure. *Annu. Rev. Fluid Mech.* **1974**, *6*, 227−255.
(39) Guo, J.; Lewis, J. A. Aggregation effects on compressive flow properties and drying behaviour of colloidal silica suspensions. *J. Am. Ceram. Soc.* **1999**, *82*, 2345.
(40) Lange, F. F.; Miller, K. T. Pressure filtration: Consolidation kinetics and mechanics. *Am. Ceram. Soc. Bull.* **1987**, *66*, 1498.
(41) Lewis, J. A. Colloidal processing of ceramics. *J. Am. Ceram. Soc.* **2000**, *83*, 2341.
(42) Russel, W. B.; Saville, A. D.; Schowalter, R. W. *Colloidal Dispersions*; Cambridge University Press: Cambridge, U.K., 1989.
(43) Peppin, S. S. L.; Huppert, H. E.; Worster, M. G. Steady-state solidification of aqueous ammonium chloride. *J. Fluid Mech.* **2008**, *599*, 465−476.
(44) Cahn, J. W.; Dash, J. G.; Fu, H. Theory of ice premelting in monosized powders. *J. Cryst. Growth* **1992**, *123*, 101.
(45) Peppin, S. S. L.; Elliott, J. A. W.; Worster, M. G. Pressure and relative motion in colloidal suspensions. *Phys. Fluids* **2005**, *17*, 053301.
(46) Ozawa, H.; Kinosita, S. Segregated ice growth on a microporous filter. *J. Colloid Interface Sci.* **1989**, *132*, 113−124.
(47) Style, R. W.; Peppin, S. S. L. The kinetics of ice-lens growth in porous media. *J. Fluid Mech.* **2012**, *692*, 482.
(48) Hansen-Goos, H.; Wettlaufer, J. S. Theory of ice premelting in porous media. *Phys. Rev. E* **2010**, *81*, 031604.
(49) Nolan, G. T.; Kavanagh, P. E. The size distribution of interstices in random packings of spheres. *Powder Technol.* **1994**, *78*, 231−238.
(50) Wilen, L. A.; Wettlaufer, J. S.; Elbaum, M.; Schick, M. Dispersion-force effects in interfacial premelting of ice. *Phys. Rev. B* **1995**, *52*, 12426.
(51) Andersland, O. B.; Ladanyi, B. *Frozen Ground Engineering*, 2nd ed.; John Wiley & Sons, Inc.: New York, 2004.